

$$\Delta_{k_1}(z_0) = (l - k) \int_{\Omega} u_k^* \frac{\partial u_1}{\partial k} dV + i(l - k) D_k(z_0) = i(l - k) [D_k(z_0) - Z_k]. \quad (\text{A21})$$

Equation (A19) is quoted in Eq. (2.20) of the text.

¹J. Friedel, *Philos. Mag.* **43**, 153 (1952); *Adv. Phys.* **3**, 446 (1954); *Ann. Phys. (Paris)* **9**, 158 (1954).

²A. Sugiyama, *J. Phys. Soc. Jap.* **15**, 965 (1960).

³D. C. Langreth, *Phys. Rev. B* **5**, 2842 (1972).

⁴For a discussion of the jellium model see, for example, N. D. Lang and W. Kohn, *Phys. Rev. B* **1**, 4555 (1970).

⁵E. I. Blount, in *Solid State Physics*, edited by F. Seitz and D. Turnbull (Academic, New York, 1962), Vol. 13, p. 305.

Inelastic Low-Energy-Electron Diffraction for Surface-Plasmon Studies: Extended Measurements on Epitaxial Al(111)*†

J. O. Porteus and W. N. Faith

Physics Division, Michelson Laboratory, China Lake, California 93555

(Received 7 December 1972)

Inelastic low-energy-electron diffraction measurements on a clean Al(111) surface have been greatly extended and improved. This provides the experimental basis for a much more accurate determination of the high-momentum surface-plasmon dispersion and lifetime. The surface is prepared *in situ* in an ultrahigh-vacuum scanning diffractometer by epitaxial deposition on a Si(111) single-crystal wafer. Specular beam inelastic intensity profiles are measured in the $\langle 11\bar{2} \rangle$ and $\langle 1\bar{1}0 \rangle$ directions at 15° and 25° incidence. The primary beam energy is chosen to correspond closely to both diffraction-before-loss and loss-before-diffraction processes involving different vestigial Bragg peaks at roughly 50 and 100 eV. Present emphasis is on loss profiles, which have recently been shown to be essentially free of complicating dynamical effects. The use of a 100-meV data grid and a more efficient computer differentiation technique permits determination of loss peak positions to 50 meV under favorable conditions. Internal consistency of the data is demonstrated here and in a more comprehensive analysis by Duke and Landman, published separately. The analysis leads to a substantially different evaluation of the surface-plasmon dispersion than previously obtained. There is evidence that the visibly smoother substrate used in the present work does not affect this result significantly. Experimental procedures and results are discussed in detail.

I. INTRODUCTION

The role of surfaces is critical in many solid-state electronic and optical applications. Device performance often depends on the physical, chemical, and geometrical features which determine the electron-density distribution at the surface. Measurable characteristics of this distribution are therefore of considerable practical interest. Surface plasmons¹ offer such a characteristic in the form of parameters defining the surface-plasmon dispersion and lifetime (SPDL). When the plasmon wave vector p_{\parallel} is small compared to the dimensions of the Brillouin zone² the SPDL may be evaluated from optical measurements. The spatial resolution for electron-density variations normal to the surface is quite limited, however, being of the order of $2\pi/p_{\parallel}$. The SPD at larger values of p_{\parallel} has been obtained from the distribution of 34-keV electrons scattered in a Mg foil,³ but the surface was not well characterized. The surface-plasmon signal using this method is often too weak for precise results.

A more promising method, which is compatible with elastic low-energy-electron diffraction (ELEED),^{4,5} Auger-electron spectroscopy,⁶ and other surface analytic tools,⁷ is based on inelastic low-energy-electron diffraction (ILEED).^{5,8-15} Here electrons having $\sim 10 - 100$ -eV energy are involved in an inversive two-step process: (a) An electron loses energy and a related momentum in exciting a surface plasmon; (b) the electron is elastically diffracted backward by the lattice. As a result, each vestigial Bragg peak in the *elastic* intensity vs energy curve (elastic energy profile) of an ELEED beam is accompanied by an *inelastic* intensity distribution which provides information on the surface plasmon. Sections of the inelastic distribution lying in the azimuth of the ELEED beam are called energy, angular, or loss profiles,^{9,11} depending on whether the primary energy E , exit (polar) angle θ' , or energy loss w , respectively, is chosen as the scanned variable; other variables, including the azimuth ψ and the incidence angle θ , remain fixed. The loss profile is now known to be the most useful data form for determination of the SPDL.^{13,14}

Except for a limitation at small p_{\parallel} ,⁸ where the optical methods are applicable, ILEED provides the SPDL to p_{\parallel} values approaching the Brillouin-zone dimensions. ILEED is, of course, restricted to samples with crystallographically ordered surfaces.

A recent extension of ILEED theory to include multiple elastic scattering, i. e., dynamical effects,¹² has placed new demands on measurement and analytical procedure.^{13,14} Except for data on nonspecular beams,¹⁶ which are more difficult to analyze, the only data suitable for determination of the SPDL has been reported by the authors.¹¹ This was obtained from the (00) beam of a thick epitaxial Al(111) film deposited on a Si(111) substrate. This work is now found to be deficient in the following respects: (i) Emphasis was placed on angular, rather than loss, profiles in which dynamical effects may be neglected; (ii) the data grid (point spacing) and precision are inadequate to take full advantage of the accuracy of the theoretical model; (iii) data is limited to a single azimuth, incidence angle, and Bragg peak, so that no check for internal consistency is possible; and (iv) except for ELEEED patterns and energy profiles, no auxiliary sample characterization has been performed.

In the present paper we report a substantially improved set of measurements. Loss profiles have been obtained with a reduction in the data grid to $\Delta w = 100$ meV (effectively 50 meV), $\Delta\theta' = 1^\circ$, and with a factor of $\sqrt{2}$ greater precision in the intensity. Moreover, data have been obtained in both the $\langle 1\bar{1}0 \rangle$ and $\langle 11\bar{2} \rangle$ azimuths of the Al(111) surface at 15° and 25° incidence. Primary energies corresponding to two different Bragg peaks in each azimuth have also been explored. Although no additional sample characterization has been performed, results from the visibly smoother substrate used here indicate no effect from large-scale roughness. Substantial refinement in the SPDL result from an enlightened interpretation of the new data. Since the principal analysis is described in the following paper,¹⁵ the present discussion is confined mainly to the discussion of experimental procedure and results.

II. THEORY

ILEED phenomena were first described over forty years ago,¹⁷ but the effects of excitation momenta, which require angular resolution $\sim 1^\circ$ for observation, were reported only recently.⁸ For the surface plasmon the positions of the intensity maxima can be understood roughly on the basis of a simple conservation-law model (CLM).^{8,11} The two-step process in this case assumes only conservation of energy and momentum parallel to the surface in the inelastic step and kinematic diffraction in the elastic step. This gives rise to a doublet structure in

the inelastic angular profiles, corresponding to the two possible directions of the surface-plasmon momentum in a given azimuth. Two doublets are predicted, one at the Bragg energy E_B , corresponding to the diffraction-before-loss (DL) process,¹⁷ and one at E_B plus the plasmon energy, corresponding to the loss-before-diffraction (LD) process.¹⁸ Using this model it is possible to translate peak positions in the angular, or loss, profiles into points on the dispersion curve.¹¹ An inherent practical limitation is the difficulty of locating true peak positions, which are influenced by overlap of the bulk-plasmon¹ peak, and by asymmetry and broadening resulting from the ELEEED energy profile, plasmon lifetime, and instrumental resolution. A more fundamental limitation is that the analysis is based on the angular or loss profile exhibiting maximum intensity with respect to primary energy. This results in a dependence on the inelastic energy profiles, which are now known to be strongly influenced by dynamical effects.¹²

A quantum-field-theory model (QFTM) of inelastic diffraction by Duke *et al.*⁹ permits detailed calculation of the various inelastic profiles. Although also based on a kinematical two-step model, this theory predicts details of the intensity modulation which cannot be adequately described in terms of the CLM. In particular, the coherence between DL and LD processes is included. In the case of the bulk plasmon this leads to the phenomenon of "side-band diffraction,"⁹ which is believed to have been experimentally observed.¹⁶ However, multiple elastic scattering, which is not included in the theory, can lead to similar effects.¹² For this reason an unambiguous extraction of the bulk-plasmon dispersion from ILEED is difficult or impossible at present. The profiles associated with the surface plasmon are much simpler, since momentum is directed along the surface plane. Here the theoretical profiles, treated as functionals of the SPDL, may be compared with the experimental profiles to determine the best fit. The resulting dispersion,¹⁰ based mainly on the Al(111) angular profiles of Porteus and Faith,¹¹ agrees essentially with that obtained from the CLM. However, the data permit a wide range of ambiguity in the dispersion parameters.^{10,13}

An extension of the theory by Duke and Landman^{12,14} to include dynamical effects leads to the important result that only the loss profiles may be treated as nearly kinematic. Here dynamical effects are found to be important only when the resolution in w and θ' are better than 50 meV and 1° , respectively. It is therefore reasonable from a theoretical standpoint to use a smaller data grid than $\Delta w = 400$ meV, $\Delta\theta' = 2^\circ$, used in the authors' original data. The essential experimental limitation is the ratio of noise to amplified collector sig-

nal for a given peak width. Economy dictates a minimum spacing such that the intensity of adjacent data points is significantly different. The effect of instrumental resolution was studied¹⁴ and found to have a negligible effect on peak positions in the loss profiles, thus permitting a direct comparison of theoretical and experimental determinations of these profiles.

III. EXPERIMENTAL PROCEDURE

A. Diffractometer

The diffractometer, which is shown schematically in Fig. 1, is a noncommercial scanning-type instrument. The electron gun contains the following elements and voltages relative to ground: an emission-stabilized tungsten hairpin-type filament 1 ($-E$ V), focusing electrode 2 ($-E - 23$ V), extractor 3 ($-E + 700$ V), anode 4 (0 V). One member of each pair of deflection electrodes 5-7 is at ground potential. The voltage on the other may be varied independently or linearly with E for accurate direction of the diffracted beam into the collector over a limited range of primary voltage E . The offset provided by the two vertical deflection pairs 6, 7 performs three functions: It permits the apparent source to be moved slightly out of the fixed horizontal plane of collector rotation to compensate for small dc perturbing fields or minor sample misorientation. It obscures the sample from the hot filament, and it provides some monochromatization. Coarse collimation is provided by a vertically elongated aperture at the end of the drift tube, while fine collimation is accomplished by the two coaxial circular apertures 8 on the front of the collector 9. These select a 2° cone of electrons emerging from a limited area of the sample 10. This cone is directed to the axial region of a tube-diaphragm retarding-field analyzer formed in part by the guard shield surrounding the Faraday cylinder. Electrons having sufficient energy to overcome the retarding voltage E_r applied to the guard shield contribute to the collector signal. E and E_r are each obtained from a well-regulated power supply (Hew-

lett-Packard 6209B) combined with auxiliary voltage regulators, which provide ± 5 -mV stability over periods of 1 h or more. The direct beam current into the collector with sample removed is typically $\sim 10^{-8}$ A with a measured energy spread of $\lesssim 1$ eV.

The sample goniometer 11 and collector rotate about the same vertical axis, which lies in the sample-surface plane. The former motion varies the angle of incidence θ , and the latter varies the exit angle θ' , both angles being measured from the sample normal. The goniometer also permits rotation about the sample normal; this varies the azimuth angle ψ , which is referenced to some arbitrary crystallographic direction in the sample-surface plane. Intensity measurements are restricted to the plane of incidence, i. e., the azimuth defined by the sample normal and incident beam. Continuous ψ and θ' rotation at normal incidence permits a rapid scan of the ELEED pattern. The sample is mounted on a high-purity niobium palette, which may be removed from the goniometer by means of the manipulating rod 12, and withdrawn to position 13 for sample preparation. The rod, which also transmits the ψ rotation to the goniometer, is controlled by rotary and thrust drives 14 and 15. All mechanical drives, including those for the θ' and θ motion, are magnetically coupled through the vacuum envelope with well-concentrated fields, permitting angular settings reproducible to within 0.2° . The electromagnets are either field compensated, or are operated intermittently to eliminate spurious beam deflection. All other parts are of non-ferromagnetic materials, principally stainless steel. A freon-cooled 6-in. Orb-Ion pump and baffle provide a field-free working vacuum at 1×10^{-10} Torr or less after bakeout. Helmholtz coils maintain the residual magnetic field in the diffraction region to less than 20 mG.

B. Sample Preparation and Orientation

Details of the sample-preparation chamber 16 used in the present study are given in Fig. 2. The sample S may be rotated 360° to face any of six available vacuum ports. These contain a focused-

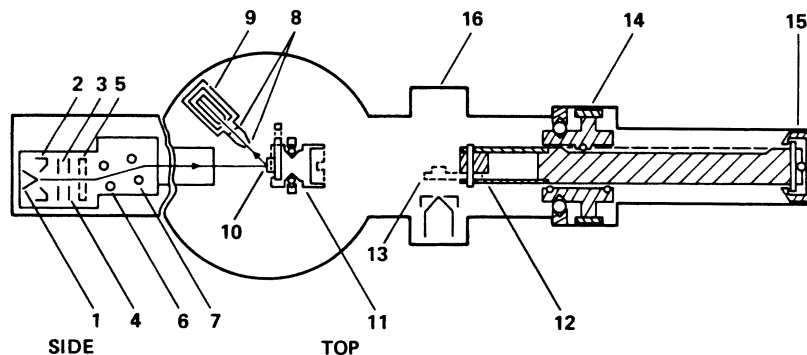


FIG. 1. Schematic of the diffractometer. The electron gun is shown rotated 90° relative to the rest of the apparatus. The goniometer 11 as shown here is set for normal incidence.

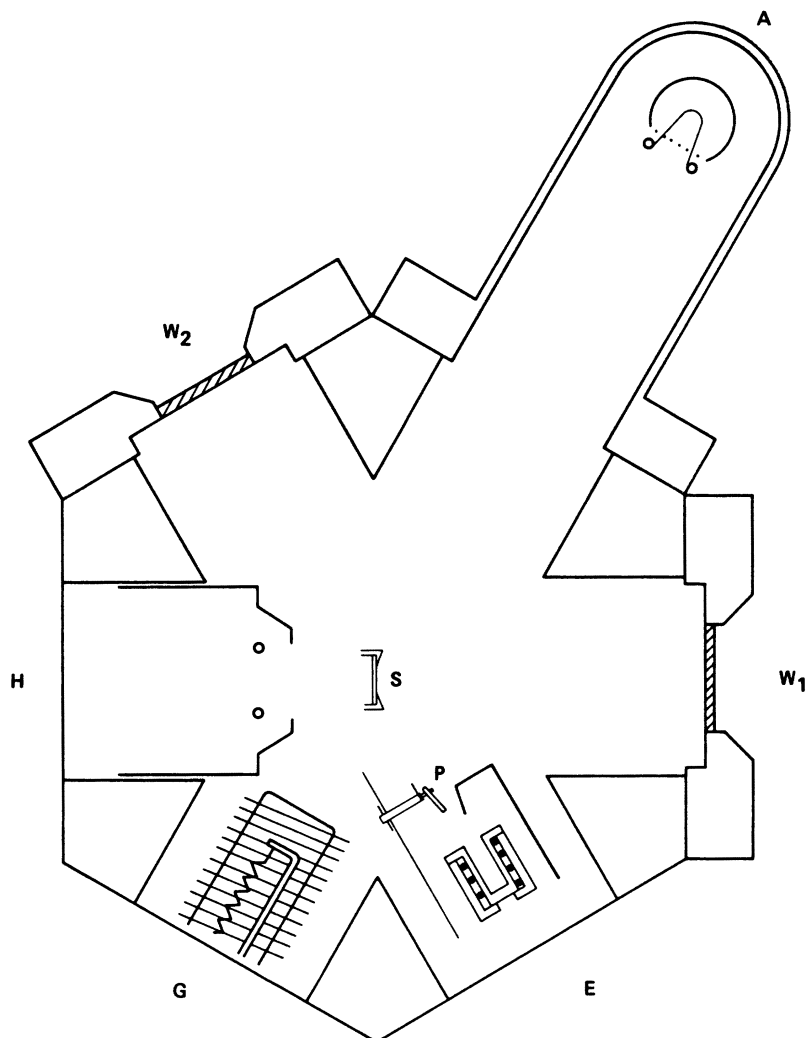


FIG. 2. Sample preparation chamber viewed toward gun end of diffractometer. The lower half of the evaporator shroud, which guides the aluminum charge into the crucible, has been omitted for clarity.

electron-bombardment heater H^{19} used only on the back surface; an ion gauge, G ; an aluminum evaporator, E ; a window, W_1 , for pyrometric measurements and for observing the sample during heating and evaporation; a residual-gas analyzer, A ; and a second window, W_2 , for observing the evaporator. The evaporator consists of a BN crucible, externally threaded to accommodate a helix of 0.010-in. tungsten heater wire, which is covered by a BN sleeve. The charge, consisting of 99.999%-pure aluminum wire, hangs on a pin, P , above the crucible until the latter has been thoroughly outgassed. The pin is then withdrawn by means of the manipulating rod 12 (Fig. 1) permitting the aluminum to drop into the crucible. Deposition rates of up to $100 \text{ \AA}/\text{min}$ can be achieved with pressures in the low 10^{-9} -Torr range as measured by the gauge. Aluminum films produced by a similar evaporator were tested for contaminants in a three-grid LEED system equipped with modulation and lock-in detection for

Auger analysis. With a sensitivity of 1% of the 67-eV aluminum Auger peak,²⁰ no contaminant peaks were observed up to the 600-eV maximum scanned energy, using 1550-eV exciting energy.

The present sample consists of an Al(111) film grown epitaxially to a thickness of $\sim 600 \text{ \AA}$ on a Si(111) single-crystal substrate. This system was studied by Lander and Morrison,²¹ and the preparation technique was developed by Bauer for energy-loss measurements.²² A new substrate (substrate No. 2) replaces the earlier one (substrate No. 1), which gave a troublesome aging effect attributed to visible changes in surface topography.¹¹ To minimize this effect the new substrate was cut from a wafer polished by the vendor, using a proprietary chemical-mechanical process. Metallurgical micrographs show little evidence of the irregularities reported on substrate No. 1. Also, no aging was apparent, but some other peculiarities were observed. In particular, good epitaxy can no longer

be obtained without heating in the initial deposition stage, although the "clean" Si(111) 7×7 pattern appears after heating to 1150°C . Also, nonspecular beams in the Al(111) ELED pattern show true six-fold intensity symmetry, indicating randomly double-positioned azimuthal orientation of epitaxial crystallites with respect to the substrate. For each day's measurement the old aluminum was re-evaporated from the substrate and a new deposition made. Measurements were normally completed within four hours of deposition; repeated data show no evidence of contamination effects at the end of this period. Further details of the preparation are given in Table I.

After deposition the sample is inserted in the goniometer and oriented for measurement. The desired ψ is first set to an accuracy of $\pm 0.5^\circ$ by adjustment of the azimuth rotation for maximum intensity of the corresponding lowest-order nonspecular ELED beam, as measured in the collector plane. The manipulating rod is then withdrawn and the incidence rotation adjusted until the (00) beam intensity is a maximum at $\theta' = \theta$, the desired angle of incidence.

C. Data Collection

The need for a highly sensitive and efficient data-collection scheme is emphasized by the new demands on precision and resolution. Accordingly, the modulation scheme used in the preceding work¹¹ was modified to a considerably more efficient com-

TABLE I. Sample preparation.

	Substrate No. 1	Substrate No. 2
Substrate material	Si, Futurecraft	Si, <i>n</i> -type, semimetals
Resistivity	50 Ωcm	1 Ωcm
Thickness	0.016 in.	0.020 in.
Surface orientation	(111) $\pm 0.005^\circ$	(111) $\pm 0.5^\circ$
Polish	abrasive	chem./mech.
Etch	1HF/3HNO ₃	1HF/3HNO ₃
Rinse	distilled water, alcohol	distilled water, alcohol
Al deposition rate	100 $\text{\AA}/\text{min}$	50 $\text{\AA}/\text{min}$
Al deposition time	6 min	12 min
Preheating	none	600°C for first minute of deposition
Anneal	400°C for 10 min after deposition	none

puter differentiation scheme.²³ The basic measurement is the retarding curve in which ψ , θ , E , θ' remain fixed while the collector signal S is measured as a function of E_r . Differentiation of this curve with respect to E_r yields essentially the loss profile. Angular profiles are derived by computer from loss profiles obtained at a sequence of equally spaced θ' values, using data points corresponding to a fixed value of E_r . Inelastic energy profiles can, in principle, be obtained in an analogous way by sequencing E instead of θ' .

Figure 3 is a flow chart of the data-collection system used to obtain retarding curves. The components, starting at the upper left and proceeding clockwise, are as follows: the collector, already described; a Cary model-36 vibrating-reed dc amplifier, which is noise limited at 1×10^{-15} A for a

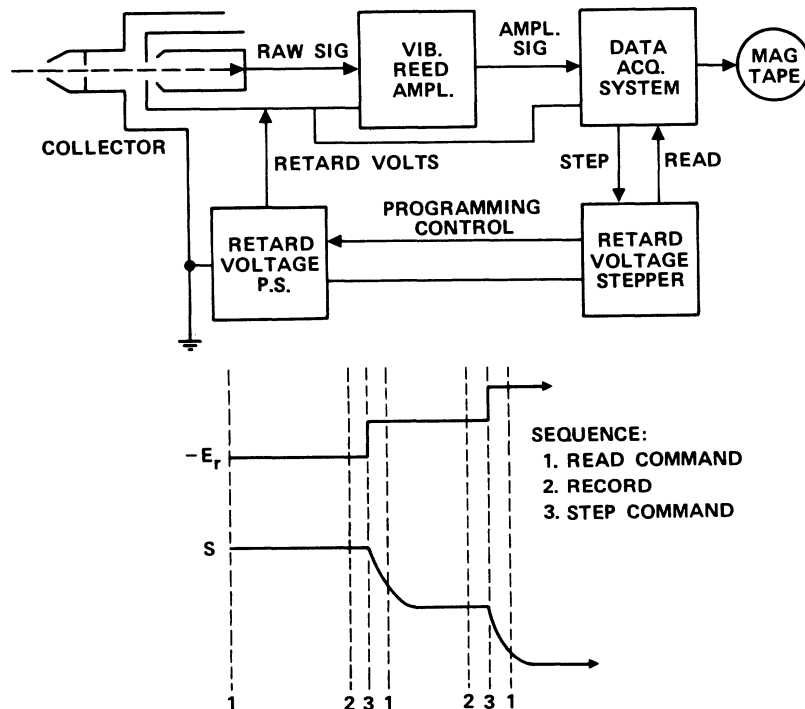


FIG. 3. Flow chart of data-collection system with timing diagram for present measurements.

0.1-sec response time; a Vidar 5203 digital-data-acquisition system (DAS), which converts the amplified analog signal to digital form and records it on magnetic computer tape; a noncommercial voltage stepper containing a programmable sequence of resistances for control of the retarding-voltage power-supply output. The stepper uses conventional scaling circuitry to step through up to 12 binary digits of resistance in a basic unit equivalent to $\Delta E_r = 100$ mV, with an over-all accuracy of better than ± 10 mV in present applications.

The operating sequence for obtaining a retarding curve is described with reference to the timing diagram at the bottom of Fig. 3. Operation starts with a manual read command 1 to the DAS. Following a delay of 0.15 sec, the collector signal at the first level of E_r is recorded at 2, after completion of which the DAS sends out a step command at 3. In response, the stepper advances E_r to the second level and generates a second read command 1. The cycle is then automatically repeated through the final preselected E_r level. At this point the scaler encounters a digit corresponding to zero control resistance, whereupon E_r returns to the first level and the entire scan is repeated. The number of scans, which is determined by the precision required, is controlled by the optional upper scaling limit. Between retarding curves the spectrometer is typically reset to the next θ' , which is done automatically on manual command, or to the beginning θ' and the next E if the angular scan is complete.

Data reduction begins with conversion of E_r to w , by requiring that $w = 0$ coincide with the elastic peak in the loss profile as discussed in Sec. III D. The inelastic intensity I per unit w is then obtained by differentiating the collector signal and averaging over the N scans, using

$$I[w_i + (2n\Delta w)^{-1}] = (Nn\Delta w S_0)^{-1} (\cos\theta'/\cos\theta) \times \sum_{j=1}^N (S_{i+n,j} - S_{i,j}), \quad (1)$$

where $S_{i,j}$ is the collector signal measured at the loss level w_i in the j th scan. The normalization factor $S_0^{-1} \cos\theta'/\cos\theta$ compensates for variations in the direct-beam collector signal S_0 with E , for variation of the collector-viewed sample area with θ' , and for variation of the irradiated area with θ . The parameter n , which determines the effective energy resolution, is equivalent to a modulation amplitude in units of the grid interval Δw . In the present scheme n may be selected as necessary after the measurement for optimum data smoothing. The flexibility in n is used to reduce the actual Δw from the minimum of 100 meV provided by the stepper to an effective Δw of 50 meV. This is possible because of the $(2n\Delta w)^{-1}$ term in the argument of I , and is achieved by superimposing the results

of two separate data reductions, where n is first set equal to an odd, and then to an even integer. Consecutive integers are used to avoid a significant difference in the effective energy resolution. Error bars corresponding to \pm the standard deviation σ_I in I accompany each data point in the computer-generated plots, where²⁴

$$\sigma_I[w_i + (2n\Delta w)^{-1}] = (n\Delta w S_0)^{-1} (N-1)^{-1/2} (\cos\theta'/\cos\theta) \times \left\{ N^{-1} \sum_{j=1}^N (S_{i+n,j} - S_{i,j})^2 - N^{-2} \left[\sum_{j=1}^N (S_{i+n,j} - S_{i,j}) \right]^2 \right\}^{1/2}. \quad (2)$$

Observe that σ_I is derived from the reproducibility of I between successive scans, and does not include systematic errors.

After each deposition and before inelastic measurements are made, the elastic energy profile of the (00) beam is always scanned. This serves as a uniformity control on the sample quality and goniometer settings, as well as providing necessary information for the SPDL analysis. The elastic intensity is taken as the collector signal with $E_r = 5.4$ V to exclude the inelastics and secondaries. With the collector positioned for maximum beam intensity the output of the amplifier is displayed in analog form on an XY recorder as a continuous function of E . A correction for variations in the direct-beam collector signal is performed manually.

D. Instrumental Resolution and Accuracy Limitations

The most critical variables in SPDL determinations are θ' and w . The absolute accuracy with which these variables may be assigned to features in the inelastic profiles is limited mainly by resolution and the effect of systematic instrumental errors. The angular resolution is determined by the combination of incident beam divergence and collector acceptance. The effective incident divergence varies as $\cos\theta/\cos\theta'$, while the collector acceptance is constant. Since the incident divergence component is relatively small ($\sim 0.5^\circ$) for the settings used here, the variation of angular resolution with θ and θ' is correspondingly small. In the specular direction, which is the most important direction for the analysis involving the (00) beam, the total angular resolution is represented by the direct-beam angular profile shown in Fig. 4. The peak of this profile determines the zero of the collector-angle scale. To evaluate the effect of systematic errors in θ' which may result from residual fields the positions of a nonspecular ELEED beam were computed from the sample lattice constant and verified by experiment. Since the beam positions depend on E and θ , the absolute accuracy

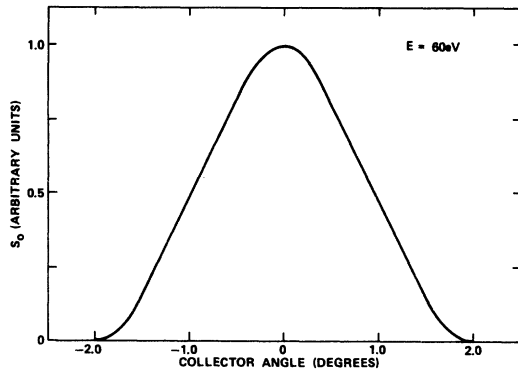


FIG. 4. Angular profile of the direct beam obtained by measuring the direct-beam collector current as a function of collector angle. The sample has been removed from the goniometer and the latter turned to avoid interference.

of these variables can also be estimated. Internal consistency indicates an absolute accuracy of better than $\pm 0.5^\circ$ in θ' and θ , and better than ± 1 eV in E .

The effective energy resolution depends on the combined effects of diffractometer resolution and the resolution $n\Delta w$ selected for data reduction. Except for a small contribution from inelastic background scattering, these determine the shape of the elastic peak in the loss profile, which is shown in Fig. 5 for $n\Delta w = 0.8$ eV. The absolute accuracy of w (± 0.1 eV) depends on how closely $w = 0$ may be chosen to coincide with this peak. The peak differs from $E_r = 0$, also shown, by 0.25 eV as a result of thermionic energy and the difference in effective surface potential of source and collector.

The relative accuracy of θ' and w are limited mainly by the signal-to-noise ratio and resolution. In practice these usually are more significant limitations than the reproducibility of the collector setting ($\pm 0.2^\circ$) or the reproducibility of the stepper-controlled retarding voltage (± 10 mV).

IV. EXPERIMENTAL RESULTS AND DISCUSSION

A. Elastic Energy Profiles

To locate ILEED structure suitable for SPDL determination one must first locate well-defined Bragg (kinematical) peaks in the elastic energy profile. Such peaks can often be identified by their persistence with changing incidence angle. The identification can be verified from theory, where dynamical features may be studied independently.^{25,26} Experimental elastic energy profiles are also important for the analysis, where they are used to characterize the theoretical elastic scattering.^{10,13}

Figure 6 shows elastic energy profiles of the (00) beam at $\theta = 15^\circ$, 25° from Al(111) films on substrate No. 2. The azimuth contains the $\langle 11\bar{2} \rangle$, and an

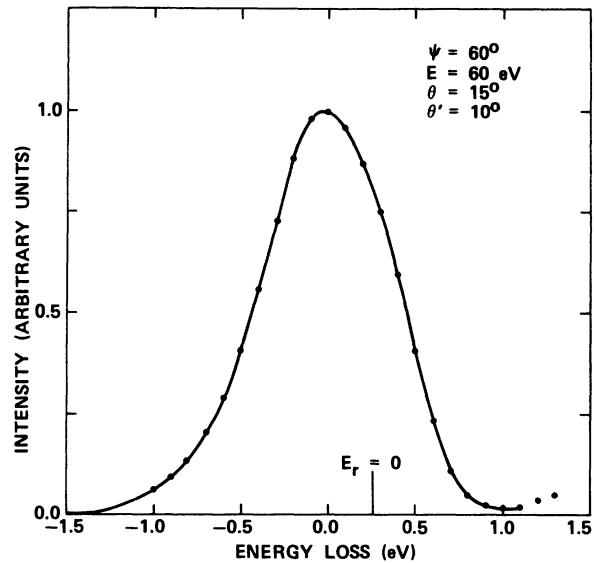


FIG. 5. Elastic peak in a typical loss profile, showing the relationship to zero energy loss.

equal mixture of $\langle \bar{1}\bar{1}2 \rangle$ direction, as a result of double positioning. These correspond in Jona's notation,²⁷ where ψ is replaced by ϕ , to $\phi = 0^\circ, 60^\circ$; these are equivalent in the (00)-beam profiles by reciprocity.²⁸ Two prominent Bragg peaks, $E_B = 49, 99$ eV, appear in the $\theta = 15^\circ$ profile. These

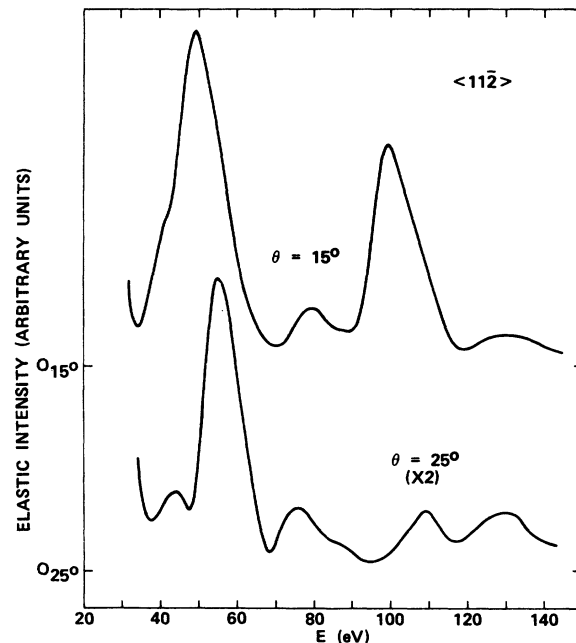


FIG. 6. Elastic energy profiles of the (00) beam from the Al(111) sample used in the present work. The azimuth corresponds to the $\langle 11\bar{2} \rangle$ or $\langle \bar{1}\bar{1}2 \rangle$ crystallographic direction.

energies are slightly lower than previously reported from substrate No. 1.¹¹ Subtle differences in peak shapes are also apparent. In the $\theta = 25^\circ$ profile the lower energy peak appears at 55 eV, while the higher energy peak is suppressed to the extent that it is not useful for precise SPDL determinations.

Figure 7 extends the above results to the $\langle 1\bar{1}0 \rangle$, or $\langle \bar{1}10 \rangle$, azimuth, i. e., the close-packed direction. This is equivalent to Jona's $\phi = 30^\circ$. Bragg peaks appear at 45 and 102 eV in the $\theta = 15^\circ$ data and at 45 and 117 eV in the $\theta = 25^\circ$ data. In general, peak positions and shapes observed here agree with those observed by Jona on single-crystal Al(111) within the combined absolute error claimed for both sets of measurements (± 6 eV).

B. Inelastic Loss Profiles

Loss profiles provide the basic data for the SPDL determinations. Choice of the best values of θ , E , and θ' for measurement depends on obtaining the most prominent and, therefore, the most precisely measurable surface-plasmon loss peaks, which are at the same time free from influences contributing to systematic error. For example, it is evident from Figs. 6 and 7 that choosing a smaller θ tends to intensify the Bragg peak and, therefore, also the inelastic structure via the role of elastic diffraction in the two-step ILEED process. On the other hand, a smaller θ also tends to enhance the excitation of

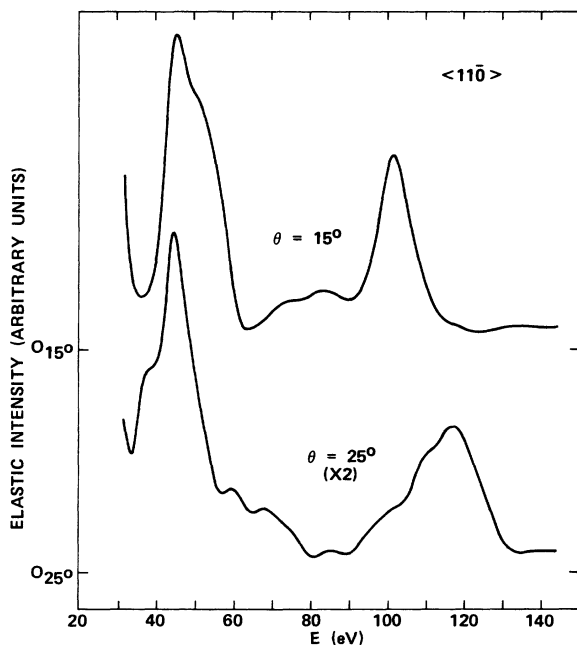


FIG. 7. Elastic energy profiles of the (00) beam from the Al(111) sample used in the present work. The azimuth corresponds to the $\langle 1\bar{1}0 \rangle$ or $\langle \bar{1}10 \rangle$ crystallographic direction.

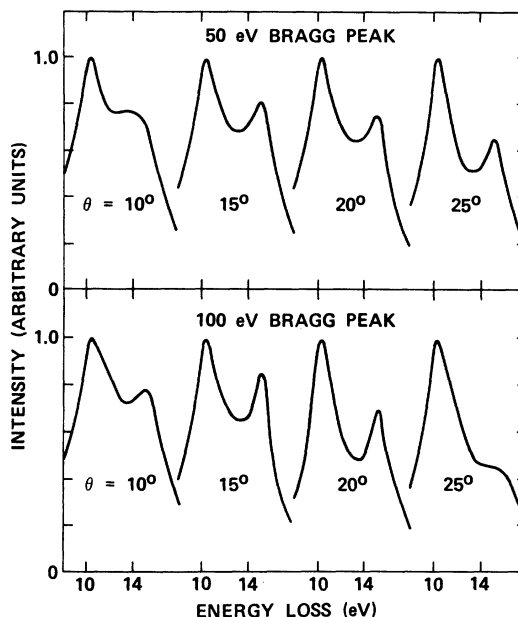


FIG. 8. Energy-loss profiles showing the relative intensity of the surface plasmon ($\omega \approx 10$ eV) to bulk plasmon ($\omega \approx 15$ eV) peaks as a function of incidence angle. The exit angle and primary energy have been selected in each case to provide the LD surface-plasmon peak with maximum intensity, shown as unity in the figure. The two pertinent Bragg peaks, nominally identified here as 50 and 100 eV, are those appearing in Fig. 6.

bulk plasmons relative to surface plasmons,¹ and thereby increases interference from the bulk-plasmon structure. This is demonstrated in Fig. 8, which shows the variation in relative intensity of the surface- and bulk-plasmon peaks in the loss profiles as a function of θ . By avoiding extreme values of θ , one can minimize the sensitivity of the SPDL analysis to uncertainties in the bulk-plasmon component, and at the same time maintain adequate intensity for precise measurement.

The intensity of the surface-plasmon loss peak as a function of E generally exhibits two maxima, one near the Bragg energy and another near the Bragg energy plus the plasmon energy. These correspond to the DL and LD processes, respectively. Although both represent favorable conditions for measurement, the larger value often produces a significantly better signal-to-noise ratio for the following reasons: (i) The LD intensity is concentrated almost entirely in one member of the predicted angular doublet, and under present conditions is greater than the DL intensity; and (ii) the elastic intensity is less than at the Bragg peak and therefore represents a smaller collector background current.

Since larger values of p_{\parallel} tend to scatter electrons at larger angles from the elastic beam, the vari-

able θ' effectively scans the plasmon momentum.¹¹ Loss profiles representing a range of θ' values including the specular direction $\theta' = \theta$ are therefore desirable. On the basis of observed inelastic intensity, values of θ' somewhat less than θ should be weighted most heavily. Possible interference from the (00) ELED beam must also be considered when measuring near the specular direction. The presence of an intense elastic component within the acceptance angle of the collector can introduce significant systematic errors⁸ in the inelastic intensity, as well as gross noise and instability.

Basic data for the QFTM analysis consists of loss profiles measured and reduced with two different sets of parameters, as follows. Coarse grid: $\Delta w = 400$ meV, $\Delta\theta' = 2^\circ$, $n = 2$, $N = 16$; fine grid: $\Delta w = 100$ meV (effective $\Delta w = 50$ meV), $\Delta\theta' = 1^\circ$, $n = 7$ and 8 , $N = 64$. In both cases $\langle 11\bar{2} \rangle$ and $\langle 1\bar{1}0 \rangle$ azimuths were explored at $\theta = 15^\circ$ and 25° . To permit more time for close spacing of data points and high precision, $E \approx E_B$ and $E \approx E_B + 10$ eV only. To provide data for a comparative CLM analysis, which requires more extensive E values, a second set of loss profiles was obtained under the following typical conditions: $\langle 11\bar{2} \rangle$; $\theta = 15^\circ, 20^\circ, 25^\circ$; $E_B - 5 \leq E \leq E_B + 20$ eV, $\Delta E = 5$ eV; $8.8 \leq w \leq 16.8$ eV, $\Delta w = 1.6$ eV; $\Delta\theta' = 2^\circ$. The modulation scheme¹¹ of data collection was used, effectively giving $n = \frac{1}{2}$, $N = 32$. Only examples from the QFTM set of data are presented and discussed here.

Figure 9 presents a series of coarse-grid loss profiles with $E \approx E_B = 49$ eV, where the DL contribution predominates. The effect of SPD is to shift the surface loss peak to larger energy loss as θ' departs from the 15° specular direction. Figure 10 presents a similar series where $E = E_B + 11$ eV, giving predominance to the LD contribution from the 49-eV Bragg peak. The greater concentration of intensity in the subspecular direction is characteristic of the LD process. Error bars representing standard deviations, which depend strongly on θ' but are statistically independent of w , are shown for one point in each curve. The greater precision in Fig. 10, as compared to Fig. 9, particularly near the specular direction, demonstrates the advantage of the reduced elastic background intensity. The remaining examples of coarse-grid data, Figs. 11–13, are offered as evidence of the internal consistency of results with changes in Bragg peak, incidence angle, and azimuth. The data are analogous in each case to that of Fig. 10 when allowance is made for variations arising from dynamical effects in the elastic diffraction and from the bulk-plasmon contribution.

The fine-grid data of Figs. 14–16 provide evidence that the dispersion-related shift of the surface loss peak is internally consistent to a much higher level of precision. Representative error

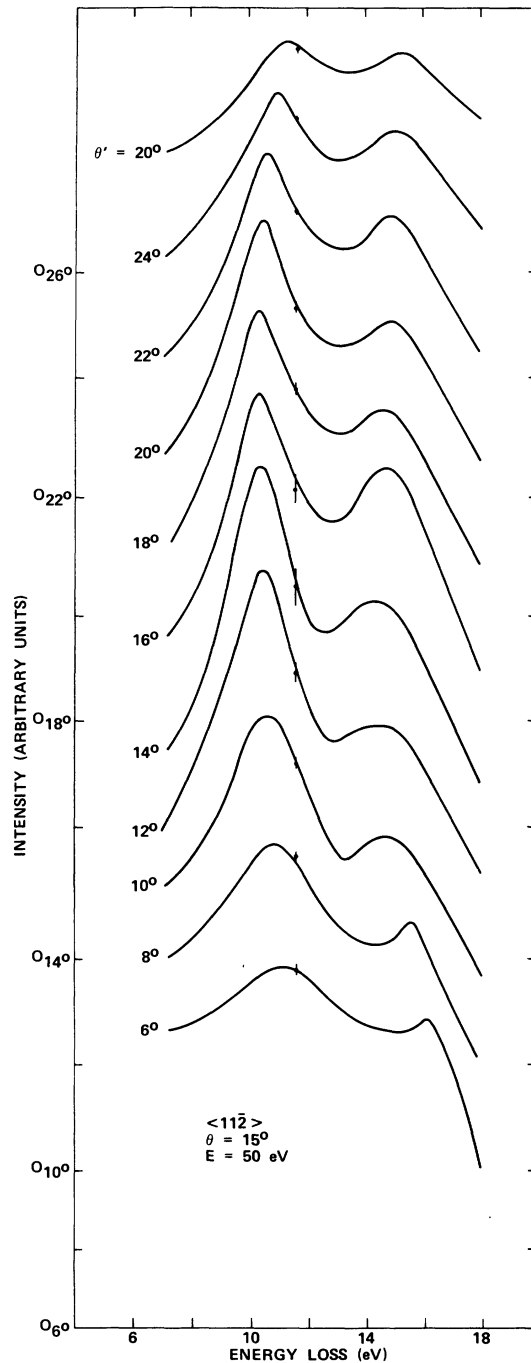


FIG. 9. Coarse grid energy-loss profiles arising predominantly from the DL process in conjunction with 49-eV Bragg peak in the upper curve of Fig. 6. The tick marks along the vertical axis indicate displaced zero levels.

bars, which are again given for each curve, are in some cases smaller than the plotted data points. To illustrate the point scatter all data points are shown for the $\theta' = 11^\circ$ curve in Fig. 15. Under

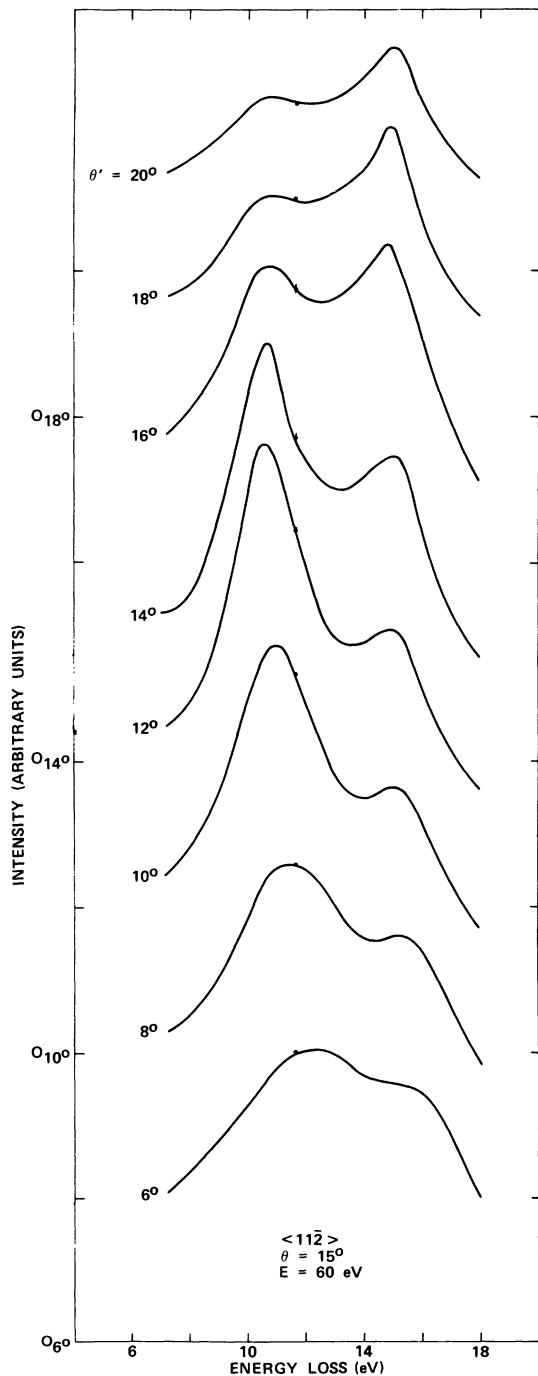


FIG. 10. Coarse grid energy-loss profiles arising predominantly from the LD process in conjunction with the 49-eV Bragg peak.

these favorable conditions relative peak positions can be determined to ± 50 meV.

C. Angular Profiles

Angular profiles provide a means of establishing the incoherent background,^{14,15} as well as providing

a check on loss-profile data. Systematic errors produced in the analyzer by an intense elastic background⁸ are strongly angle dependent and often can be more easily recognized here than in the corresponding loss profiles. The presence of substantial dynamical effects makes the angular profiles relatively unsatisfactory for SPDL determinations using

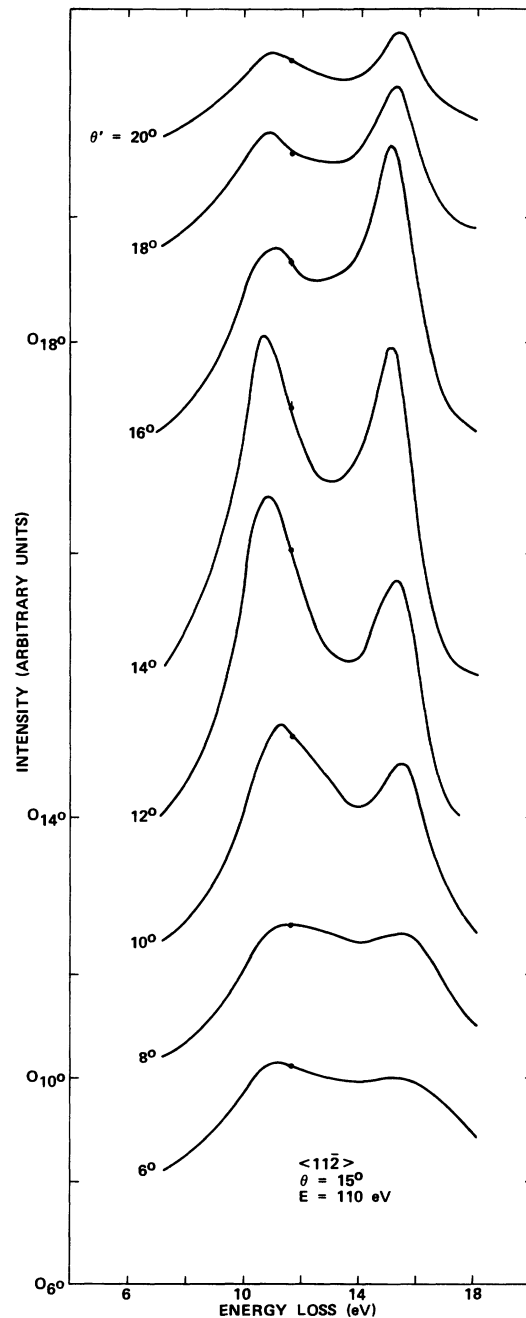


FIG. 11. Coarse grid energy-loss profiles associated with the 99-eV Bragg peak with the LD process predominant.

a kinematic analysis. Ignorance of this fact and consequent misinterpretation of the data has led to erroneous determination of the SPDL in earlier work.^{10,11}

Figure 17 presents the data of Fig. 10 in angular profile form. The displayed structure may be interpreted qualitatively in the following way. As a

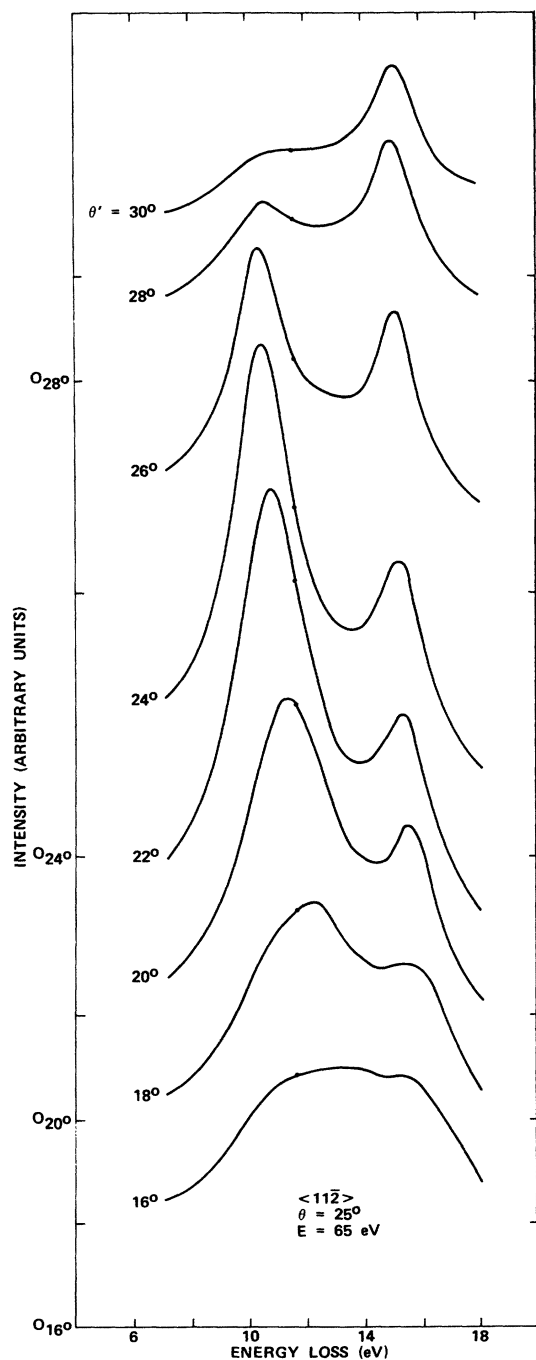


FIG. 12. Coarse grid energy-loss profiles at $\theta = 25^\circ$. The LD process from the 55-eV Bragg peak predominates.

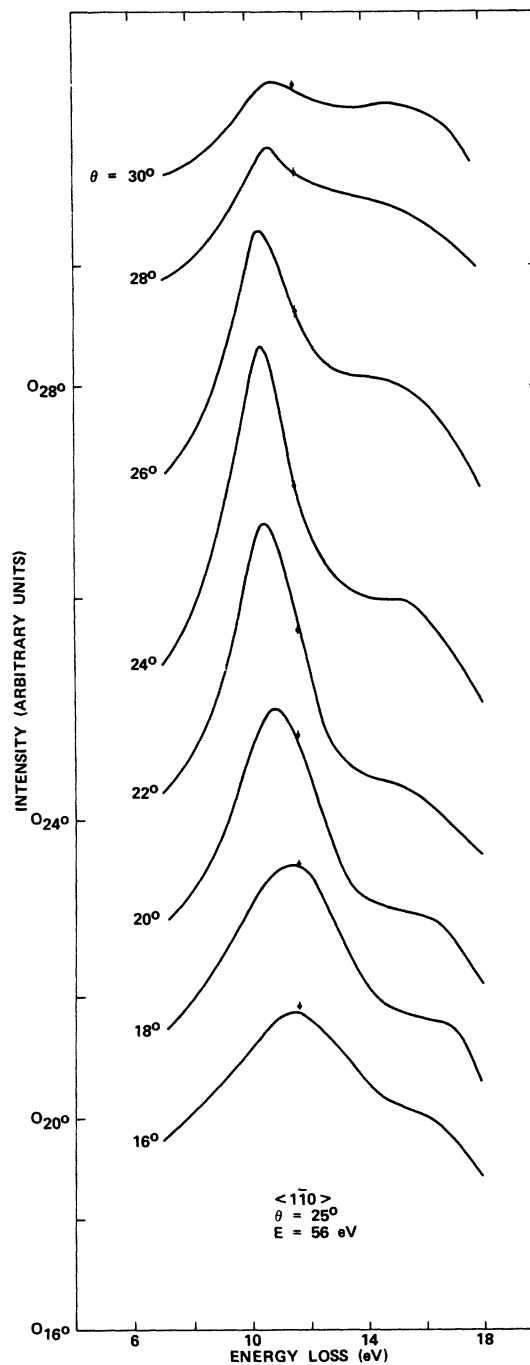


FIG. 13. Coarse grid energy-loss profiles in the $\langle 1\bar{1}0 \rangle$ azimuth at $\theta = 25^\circ$. The LD process from the 45-eV Bragg peak of Fig. 7 predominates.

result of lifetime broadening the surface-plasmon peak appears at the bottom of the figure, at loss values well below the minimum accessible plasmon energy.⁸ Proceeding upward, the peak grows with little change in angle until the minimum energy is reached near $E = 10.4 \text{ eV}$. Beyond this point the

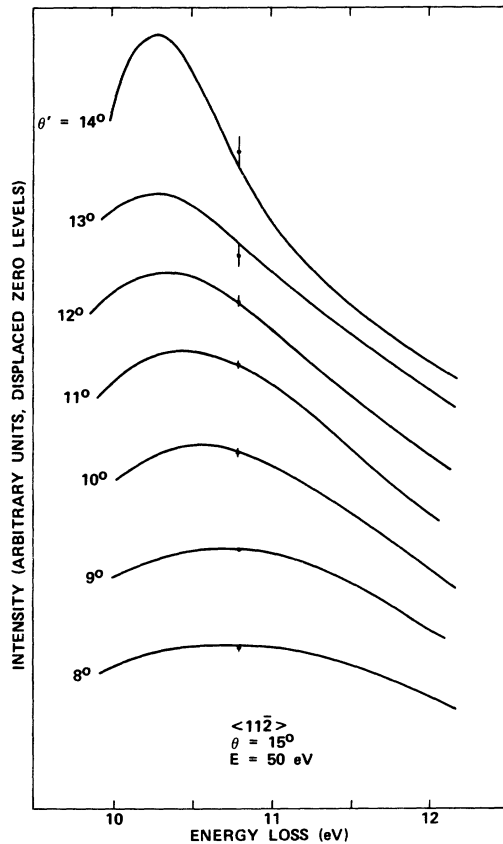


FIG. 14. Fine grid energy-loss profiles corresponding to Fig. 9.

peak shifts to smaller angles with increasing p_{11} , and diminishes in intensity as a result of the diminishing lifetime. The new peak appearing near the 15° specular direction for $w \geq 12.8$ eV is the principal bulk-plasmon peak. A third peak which appears at lower angles in this range of w apparently is also associated with the bulk plasmon, but is dynamical in origin. In earlier evaluations of the SPDL the low-angle peak was interpreted as the extension of the surface-plasmon peak to large values of w . The earlier interpretation is not supported by the more extensive loss-profile data now available. Although a corresponding low-angle peak is visible in the loss profiles at $\theta' \leq \theta - 10^\circ$, it is clearly separate from the surface-plasmon component, which can be simultaneously identified at lower values of w .

Since extensive loss-profile data similar to that reported here for substrate No. 2 is unavailable for substrate No. 1, angular profiles provide the only equivalent basis for comparing the two substrates. Comparisons were made under the following conditions: $\langle 11\bar{2} \rangle$ azimuth; $\theta = 15^\circ$; $E = 50, 55, 60$ eV; $w = 8.4-18.4$ eV, $\Delta w = 2$ eV; $\theta' = 0^\circ-30^\circ$ ($\Delta\theta' = 2^\circ$).

In all cases corresponding peaks whose position agrees to within 1° were found. This is well within the combined uncertainty of the two sets of data.

D. Surface-Plasmon Dispersion and Lifetime

The SPDL derived from the present data is significantly different from that previously reported.^{10,11} The principal reason for this is related to the reinterpretation of the *angular* profiles, particularly the disassociation of the dynamical low-angle peak from the surface plasmon. Confining the analysis to the *loss* profiles effectively forces this condition since dynamical influences are largely eliminated. Since exclusion of the low-angle peak represents a loss of information at large w , the present results depend much more heavily on the information available at small w . The demands on precision in both data and theory are therefore much greater than previously realized.

The QFTM analysis of data reported in the present work is presented in the following paper. The SPD most consistent with the available data is

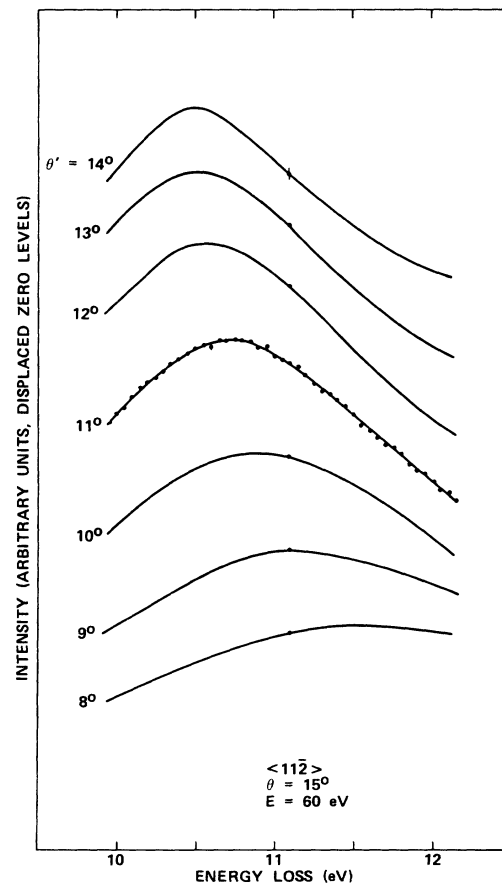


FIG. 15. Fine grid energy-loss profiles corresponding to Fig. 10.

$$\hbar\omega_s = 10.5 \pm 0.1 + (2 \pm 1)p_{\parallel} + (0.0_{-0}^{\pm 2})p_{\parallel}^2, \quad (3)$$

where $\hbar\omega_s$ is in eV and p_{\parallel} in \AA^{-1} . The corresponding lifetime \hbar/Γ_s , expressed in terms of the damping Γ_s , is found to be

$$\Gamma_s = 1.85 \pm 0.5 + (3 \pm 2)p_{\parallel}, \quad (4)$$

where Γ_s is in eV. Comparison with earlier results shows the SPD given by Eq. (3) to be much flatter as p_{\parallel} increases from zero.¹⁵

The flatter SPD and internal consistency of the data are supported by the CLM within its more severe accuracy limitations. Because of the large Δw grid in the data available for this type of analysis and the restriction of pertinent information to small w , the evaluation of p_{\parallel} is carried out for $\hbar\omega_s = 12$ eV only. To maximize accuracy and minimize the dependence on dynamical peculiarities of the inelastic energy profile the following procedure is used: All loss profiles exhibiting a prominent surface-plasmon LD maximum at $w = 12$ eV are selected from the appropriate set of data. Equation (10) of Ref. 11 is applied directly to the parameters

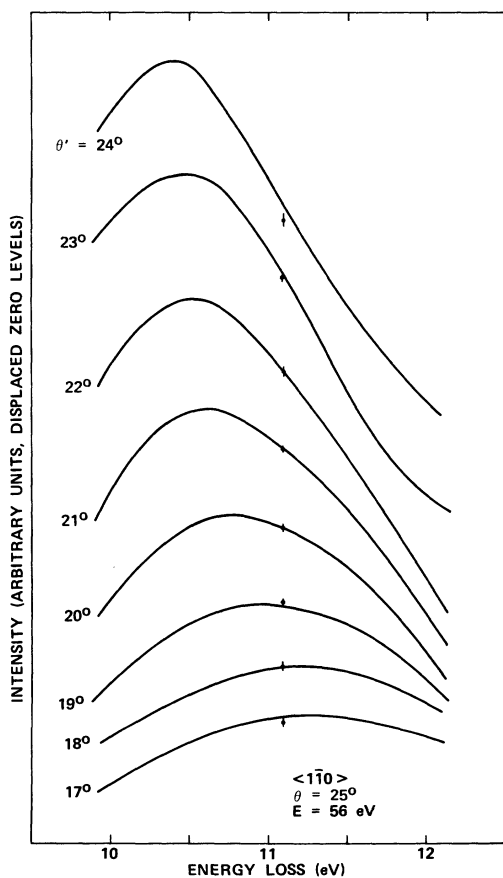


FIG. 16. Fine grid energy-loss profiles corresponding to Fig. 13.

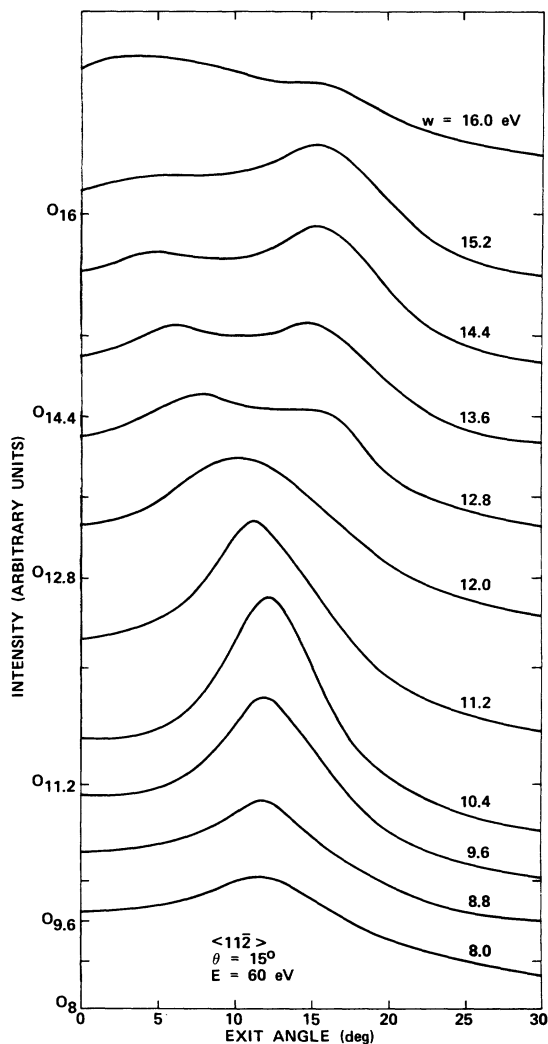


FIG. 17. Coarse grid angular profiles derived from the loss profiles of Fig. 10. The energy-loss grid has been increased from 0.4 to 0.8 eV for presentation clarity. The tick marks along the vertical axis indicate displaced zero levels.

associated with these profiles to obtain p_{\parallel} (formerly K). Extreme values for each of six available combinations of E_B and θ are used to define six individual ranges of admissible p_{\parallel} values. Results are given in Table II. The existence of a range common to all six of the individual ranges allows internal consistency within the $\langle 11\bar{2} \rangle$ azimuth. Although the common range does not contain the most probable QFTM result, it does fall well within the range of uncertainty. This minor discrepancy is due in part to the inclusion in the QFTM analysis of information from the less prominent LD peaks, which have not been included in the CLM analysis. These peaks, which occur in the range $\theta' > \theta$ often indicate a flatter dispersion than the more intense

TABLE II. Comparison of models ($\hbar\omega_s = 12$ eV).

Model	$p_{ }$ range designation	E_B (eV)	θ (deg)	Range	
				min $p_{ }$ (\AA^{-1})	max $p_{ }$ (\AA^{-1})
CLM	individual	49	15	0.55	0.78
CLM	individual	99	15	0.51	0.69
CLM	individual	52	20	0.46	0.59
CLM	individual	106	20	0.53	0.70
CLM	individual	55	25	0.47	0.70
CLM	individual	107	25	0.55	0.73
CLM	over-all			0.46	0.78
CLM	common			0.55	0.59
QFTM	most probable			0.75	
QFTM	uncertainty			0.37	1.6

peaks at $\theta' < \theta$.¹⁵ The neglect of bulk-plasmon overlap in the CLM may also be significant. In general, the QFTM result represents a much larger body of data, including both DL and LD processes, as well as two azimuths. The CLM results therefore can be expected only to form a subset of the QFTM uncertainty range,¹⁵ which Table II clearly shows to be the case.

An additional consideration in comparing Eqs. (3) and (4) with the previously reported SPDL is the role of surface roughness. It is conceivable that the effect of roughness contouring on the electron-density distribution at the surface has a significant influence on both dispersion and lifetime. Since substrate No. 1 exhibits visible irregularities which were not evident on substrate No. 2, it might be expected that results for the two substrates would be substantially different. Unfortunately, the extensive loss-profile data, required to perform an accurate analysis on substrate No. 1, is lacking. Since the previously reported analyses^{10,11} were largely based on data features now tentatively associated with the bulk plasmon, this type of result has little relevance to surface roughness. The only pertinent basis for comparison of the two substrates is the surface-plasmon peak in the limited angular profile data previously discussed. From the lack of evidence for any significant discrepancy in the position of this peak, we conclude that the SPD determined from ILEED is relatively insensitive to visible long-range irregularities. The SPD may, however, be sensitive to irregularities on a much smaller scale. This can only be determined by fu-

ture experiments on surfaces with carefully controlled short-range irregularities.

V. SUMMARY

ILEED measurements near the (00) elastic beam from epitaxial Al(111) have been extended and improved, with precise determination of the surface-plasmon dispersion and lifetime as the principal objective. Emphasis has been shifted from angular to loss profiles in view of the latter's predominant kinematic property as demonstrated in recent theoretical work. A smaller data grid and more efficient data-collection procedure provides a significant improvement in signal-to-noise ratio and resolution. Under favorable conditions the relative position of energy-loss peaks can be located to within 50 meV with 2° angular resolution. Measurements have been extended to include two different Bragg peaks, two angles of incidence, and two crystallographic directions. The analysis has shown these to be largely consistent, yielding internally consistent results for the surface-plasmon dispersion and lifetime. These results differ from those previously reported on the basis of more limited and less precise data. The difference is mainly attributable to an enlightened interpretation of the new data resulting from new theoretical results. The use of a visibly smoother substrate evidently has little influence, although sensitivity to short-range roughness cannot be excluded on the basis of present work. Further ILEED measurements on surfaces with controlled irregularities on a lateral scale of 100 \AA or less are needed to explore this. Measurements on other crystallographic faces and an investigation of the influence of chemisorbed layers on the SPDL would also be of considerable interest.

ACKNOWLEDGMENTS

The authors are indebted to Dr. C. B. Duke and Dr. E. Bauer for critical readings of the manuscript and for many helpful suggestions; to Dr. Duke and Dr. U. Landman for their close cooperation in analyzing present results; to Dr. G. E. Laramore for stimulating discussions; and to Maxine J. Booty for development of the computer programs used in data reduction and plotting.

*Work supported in part by the Defense Advanced Research Projects Agency under Order No. 2175 and in part by Navy Independent Research funding.

¹H. Raether, *Ergeb. Exakten Naturwiss.* **38**, 84 (1965).

²N. Marschall, B. Fischer, and H. J. Queisser, *Phys. Rev. Lett.* **27**, 95 (1971); B. Fischer, N. Marschall, and H. J. Queisser, *Surf. Sci.* **34**, 50 (1973).

³C. Kunz, *Z. Phys.* **196**, 311 (1966).

⁴P. J. Estrup and E. G. McRae, *Surf. Sci.* **25**, 1 (1971).

⁵G. E. Laramore, *J. Vac. Sci. Technol.* **9**, 625 (1972).

⁶C. C. Chang, *Surf. Sci.* **25**, 53 (1971).

⁷C. B. Duke and R. L. Park, *Phys. Today* **25** (8), 23 (1972).

⁸J. O. Porteus, in *The Structure and Chemistry of Solid Surfaces*, edited by G. Somorjai (Wiley, New York, 1969), p. 12; J. O. Porteus and W. N. Faith, *Phys. Rev. B* **2**, 1532 (1970).

⁹C. B. Duke, G. E. Laramore, and V. Metzger, *Solid State Commun.* **8**, 1189 (1970); C. B. Duke, A. J. Howsman, and G. E. Laramore, *J. Vac. Sci. Technol.* **8**, 10 (1971); C. B. Duke and G. E. Laramore, *Phys. Rev. B* **3**, 3183 (1971); G.

- E. Laramore and C. B. Duke, *Phys. Rev. B* **3**, 3198 (1971).
- ¹⁰A. Bagchi, C. B. Duke, P. J. Feibelman, and J. O. Porteus, *Phys. Rev. Lett.* **27**, 998 (1971); C. B. Duke and A. Bagchi, *J. Vac. Sci. Technol.* **9**, 738 (1972); A. Bagchi and C. B. Duke, *Phys. Rev. B* **5**, 2784 (1972).
- ¹¹J. O. Porteus and W. N. Faith, *J. Vac. Sci. Technol.* **9**, 1062 (1972).
- ¹²C. B. Duke and U. Landman, *Phys. Rev. B* **6**, 2956 (1972); C. B. Duke and U. Landman, *Phys. Rev. B* **6**, 2968 (1972).
- ¹³C. B. Duke, U. Landman, and J. O. Porteus, *J. Vac. Sci. Technol.* **10**, 183 (1973).
- ¹⁴C. B. Duke and U. Landman, *Phys. Rev. B* **7**, 1368 (1973).
- ¹⁵C. B. Duke and U. Landman, following paper, *Phys. Rev. B* **8**, 505 (1973).
- ¹⁶J. M. Burkstrand and F. M. Propst, *J. Vac. Sci. Technol.* **9**, 731 (1972); J. M. Burkstrand, *Phys. Rev. B* **7**, 3443 (1973).
- ¹⁷C. Davison and L. H. Germer, *Phys. Rev.* **30**, 705 (1927).
- ¹⁸J. C. Turnbull and H. E. Farnsworth, *Phys. Rev.* **54**, 507 (1938).
- ¹⁹C. F. Hempstead, Ph.D. thesis (Cornell University, 1955), pp. 9 and 10 (unpublished).
- ²⁰D. T. Quinto and W. D. Robertson, *Surf. Sci.* **27**, 645 (1971).
- ²¹J. L. Lander and J. Morrison, *Surf. Sci.* **2**, 553 (1964).
- ²²E. Bauer, NASA Annual Report for Period 1, NASA Contract No. R-05-030-001, April 1969 (unpublished).
- ²³B. Feuerbacher and B. Fitton, *Rev. Sci. Instrum.* **42**, 1172 (1971).
- ²⁴See, for example, L. G. Parratt, *Probability and Experimental Errors in Science* (Wiley, New York, 1961), pp. 92-94.
- ²⁵G. E. Laramore and C. B. Duke, *Phys. Rev. B* **5**, 267 (1972).
- ²⁶D. W. Jepsen, P. M. Marcus, and F. Jona, *Phys. Rev. B* **6**, 3684 (1972).
- ²⁷F. Jona, *IBM J. Res. Dev.* **14**, 444 (1970).
- ²⁸M. G. Lagally, T. C. Ngoc, and M. B. Webb, *Surf. Sci.* **25**, 444 (1971).

Surface-Plasmon Dispersion in Al(111) Films

C. B. Duke and U. Landman

Xerox Research Laboratories, Rochester, New York 14644

(Received 7 December 1972)

The extraction of the surface-plasmon dispersion relation from experimentally measured inelastic low-energy- ($20 \lesssim E \lesssim 200$ eV) electron diffraction intensities on Al(111) films is described. Our analysis is based on the two-step model of inelastic diffraction. Attention is focused on the methodology of determining the model parameters from the data analyses, the internal consistency of parameters obtained from the consideration of independent data, and the accuracy of the values of the parameters as determined using our procedure. Examination of eight independent sets of experimental intensities leads to the dispersion relation $\hbar\omega_s(p_{\parallel}) = 10.5(\pm 0.1) + 2(\pm 1)p_{\parallel} + 0(+2)p_{\parallel}^2$; $\Gamma_s(p_{\parallel}) = 1.85(\pm 0.5) + 3(\pm 2)p_{\parallel}$, for energies measured in eV and momenta in \AA^{-1} .

I. INTRODUCTION

The principal thrust of modern surface spectroscopy is the determination of the chemical, geometrical, vibrational, and electronic structure of the upper few layers of a solid in a high-vacuum environment.¹ The three major techniques for determining those features of the electronic excitation spectra associated with solid surfaces are inelastic low-energy-electron diffraction (ILEED), ion-neutralization spectroscopy (INS), and photoelectron spectroscopy (PES). In a previous paper² we constructed a procedure for analyzing ILEED intensity data to extract from them the dispersion relation of electronic surface excitations. Herein we apply this procedure to determine, from data taken by Porteus and Faith,³ the dispersion relation of surface plasmons⁴ at the vacuum interface of Al(111). Our results,

$$\hbar\omega_s(p_{\parallel}) = 10.5(\pm 0.1) + 2(\pm 1)p_{\parallel} + 0(+2)p_{\parallel}^2, \quad (1a)$$

$$\Gamma_s(p_{\parallel}) = 1.85(\pm 1) + 3(\pm 2)p_{\parallel}, \quad (1b)$$

already have been reported.⁵ In Eqs. (1) $\hbar\omega_s(p_{\parallel})$ is the real part of the energy of the surface plasmon measured in eV as a function of its wave number \vec{p}_{\parallel} for motion parallel to the surface measured in \AA^{-1} . The quantity $\Gamma_s(p_{\parallel})$, also measured in eV, is the imaginary part of this energy, which provides a measure of the lifetime of the surface plasmon. These results supersede those based on an earlier study by Bagchi and Duke⁶ of a more limited range of data. In this paper we describe the analysis from which Eqs. (1) were obtained and compare it with the previous one.⁶ We proceed in two steps. First, in Sec. II we review the definition² of our analytical procedure, and dispense with a few preliminary items such as the selection of data and the distinction between inelastically diffracted beams and the incoherent background on which they are superposed. Then, in Sec. III we describe our analysis of the selected ILEED intensities. We conclude our presentation with a brief synopsis in Sec. IV.